Dynamical dimer-dimer correlation functions from exact diagonalization

Ralph Werner
Physics Department, University of Wuppertal, D-42097 Wuppertal, Germany and
Physics Department, Brookhaven National Laboratory, Upton, NY 11973-5000
(February 1, 2008)

Preprint. Typeset using REVTEX

A regularization method is presented to deduce dynamic correlation functions from exact diagonalization calculations. It is applied to dimer-dimer correlation functions in quantum spin chains relevant for the description of spin-Peierls systems. Exact results for the XY model are presented. The analysis draws into doubt that the dimer-dimer correlation functions show the same scale invariance as spin-spin correlation functions. The results are applied to describe the quasi-elastic scattering in $CuGeO_3$.

I. INTRODUCTION

Dynamical correlations characterize the spectral properties of physical systems. They are accessible by a multitude of experimental setups. Even static properties such as correlation lengths extracted from energy integrating methods such as X-ray scattering also require the theoretical knowledge of the dynamics of the correlations to allow for comparison. The access to dynamical correlation functions for physically relevant systems is usually difficult even in exactly solvable models.[1–3] Dynamical spin-spin correlation functions in Heisenberg chains have been widely studied numerically[4,5] as well as analytically.[6–8]

Usually the focus lies on the imaginary part of the correlation functions. The real and the imaginary parts can be Kramers-Kronig transformed into each other and thus hold the same information. The information that can be extracted from finite systems accessible by exact diagonalization (ED) concerning the thermodynamic limit is limited. The accuracy of the results is different for different regions of the spectrum. In the case of finite systems it proves thus useful to actually calculate both quantities to extrapolate to the thermodynamic limit. The emphasis of this article lies on the presentation of a method to accurately extract the real part of the correlation functions.

The random-phase-approximation (RPA) approach applied by Cross and Fisher[9] to describe the spin Peierls-transition has been successfully applied to $CuGeO_3$.[10–14] To compare with neutron or X-ray scattering data the phononic dynamic structure factor has to be determined.

$$S(\mathbf{q},\omega) = -\frac{1}{\pi}\frac{\sum_\nu \mathrm{Im} D_\nu(\mathbf{q},\omega)}{1-\exp(-\beta\omega)} \tag{1}$$

ν labels the relevant phonon modes. The retarded normal coordinate propagator $D_\nu(\mathbf{q},\omega)$ has been calculated including the spin-phonon coupling term in RPA and depends crucially on the dimer-dimer correlation function $\chi(\mathbf{q},\omega)$.

$$D_\nu(\mathbf{q},\omega) = \frac{D^{(0)}_\nu(\mathbf{q},\omega)\left(1-\chi(\mathbf{q},\omega)\sum\limits_{\nu'\neq\nu} g_{\nu',\mathbf{q}} g_{\nu',-\mathbf{q}}\, D^{(0)}_{\nu'}(\mathbf{q},\omega)\right)}{1-\chi(\mathbf{q},\omega)\sum_{\nu'} g_{\nu',\mathbf{q}} g_{\nu',-\mathbf{q}}\, D^{(0)}_{\nu'}(\mathbf{q},\omega)} \tag{2}$$

The spin-phonon coupling constants are denoted $g_{\nu',\mathbf{q}}$ and the unperturbed normal coordinate propagator is $D^{(0)}_\nu(\mathbf{q},\omega)$. Especially the real part of $\chi(\mathbf{q},\omega)$ is of relevance since it determines dominantly the poles of the phononic correlation function.[10,11,13] This dependence is the initial motivation for an accurate determination of the dimer-dimer correlation function as presented here.

The RPA-calculations predict for $CuGeO_3$ the appearance of spectral weight in the center of the phononic spectrum as a precursor of the phase transition.[10,13] I use the numerical results to discuss the temperature dependent intensity of the predicted precursor in neutron[15,16] and X-ray[17] scattering experiments. Also, the resulting description of the phonon hardening is consistent with experiment.[18]

The relevant spin-phonon coupled Hamiltonian for spin-Peierls systems consists of three parts $H = H_s + H_p + H_{sp}$. Of relevance here is the Heisenberg spin-chain Hamiltonian

$$H_s = J \sum_{\mathbf{l}} \mathbf{S}_{\mathbf{l}}\cdot\mathbf{S}_{\mathbf{l}+\hat{z}} + J_2 \sum_{\mathbf{l}} \mathbf{S}_{\mathbf{l}}\cdot\mathbf{S}_{\mathbf{l}+2\hat{z}} \tag{3}$$

with the superexchange integrals J and J_2 between nearest-neighbor (NN) and next-nearest-neighbor (NNN) magnetic ions, respectively, and spin 1/2 operators $\mathbf{S}_{\mathbf{l}}$ at magnetic ion site $\mathbf{l}$ in the three-dimensional lattice. $\hat{z}$ is a unit vector along the spin-chain direction. For a detailed discussion of the harmonic phonon part H_p and the spin-phonon coupling term H_{sp} please refer to Ref. 12.

Defining the Fourier transform of the dimer operators

$$Y_{-\mathbf{q}} := \sum_{\mathbf{l}} e^{i\mathbf{q}\mathbf{R}_{\mathbf{l}}}\, \mathbf{S}_{\mathbf{l}}\cdot\mathbf{S}_{\mathbf{l}+\hat{z}}\,, \tag{4}$$

the dimer-dimer correlation function can be written as

$$\chi(q_z, i\omega_n) = -\frac{1}{N}\int_0^\beta d\tau\; \mathrm{e}^{i\omega_n\tau}\; \langle Y_{\mathbf{q}}(\tau) Y_{-\mathbf{q}}(0)\rangle \tag{5}$$

with Matsubara frequencies $\omega_n = 2\pi n/\beta$, inverse temperature $\beta = 1/(k_{\rm B}T)$, and number of unit cells N. It depends only on momenta q_z along the spin chains. It has been calculated in the analytically continuted form, where $i\omega_n \to \omega + i\epsilon$ with $\epsilon \to 0$, by Cross and Fisher[9] with bosonization techniques as

$$\chi_{\rm CF}(q_z,\omega) = \frac{-\chi_0(\frac{k_{\rm B}T}{J})}{0.35\,k_{\rm B}T}\; I_1\left[\frac{\omega - v_s|q_z - \frac{\pi}{c}|}{2\pi k_{\rm B}T}\right]\; I_1\left[\frac{\omega + v_s|q_z - \frac{\pi}{c}|}{2\pi k_{\rm B}T}\right] \tag{6}$$

with the spin-wave velocity v_s, lattice constant c along the magnetic chains, and the functions

$$I_1(k) = \frac{1}{\sqrt{8\pi}}\;\frac{\Gamma(\frac{1}{4} - \frac{1}{2}ik)}{\Gamma(\frac{3}{4} - \frac{1}{2}ik)}. \tag{7}$$

The result has the general form of spin correlation functions obtained from conformal field theory.[8,7] I set $\hbar = 1$ in this paper.

The prefactor $\chi_0(k_{\rm B}T/J)$ is assumed constant in field theory but has been shown by Raupach *et al.* using density matrix renormalization group (DMRG) studies to be temperature dependent in the static case and for $q_z = \pi/c$,[19] where c is the lattice constant along the magnetic chains. This wave vector describes the lattice modulation in the spin-Peierls phase and is thus the relevant one for this paper. I will now turn to the question of how far the dynamical properties of the correlation function are correctly described by the field-theoretical result Eq. (6).

II. REGULARIZATION

The correlation function can be calculated after the diagonalization of the spin Hamiltonian in the spectral representation since eigenfunctions $|n\rangle$ and eigenvalues E_n are known. All numerical results in this paper are obtained using periodic boundary conditions. Defining the matrix elements

$$V_{nm} = \langle n\,|Y_{q_z}|\,m\rangle \tag{8}$$

and the Boltzmann factor

$$f_{nm}(\beta) = \frac{1}{Z}(\mathrm{e}^{-\beta E_n} - \mathrm{e}^{-\beta E_m}), \tag{9}$$

where Z is the partition function, one can write

$$\mathrm{Re}\,\chi(q_z,\omega) = \lim_{\epsilon\to 0}\sum_{m,n}\frac{f_{nm}(\beta)\,|V_{nm}|^2(\omega + E_n - E_m)}{(\omega + E_n - E_m)^2 + \epsilon^2}, \tag{10}$$

$$\mathrm{Im}\,\chi(q_z,\omega) = -\pi\sum_{m,n} f_{nm}(\beta)\,|V_{nm}|^2\;\delta(\omega + E_n - E_m). \tag{11}$$

Since real and imaginary part of the correlation function are Kramers-Kronig related via

$$\mathrm{Im}\,\chi(q_z,\omega) = -\frac{1}{\pi}\,\mathrm{P}\int_{-\infty}^{\infty}\frac{\mathrm{Re}\,\chi(q_z,\omega')}{\omega' - \omega}\,d\omega', \tag{12}$$

it suffices in principle to know one of them, or, in other words, both parts contain the full information on the correlation function. Since the diagonalization of the Hamiltonian usually is limited to finite system sizes the information that can be extracted concerning the thermodynamic limit is limited. In that case it proves useful to actually calculate both quantities. Note that for $\mathrm{Im}\,\chi(q_z,\omega)$ to have a cut off, i.e., the correlation function has a finite spectrum, $\mathrm{Re}\,\chi(q_z,\omega)$ must change sign as a function of ω.

The spectra of finite systems are discrete and thus the correlation functions Eqs. (10) and (11) contain a series of poles as a function of ω at frequencies $\omega_{nm} = E_m - E_n$. In order to extract information on the correlation function in the thermodynamic limit, i.e., $N \to \infty$, one has to distinguish between well defined quasi-particle spectra and those where interaction induces transitions between many states. In the XY case excitations of the non-interacting spin-less fermions form a well defined continuum in the $N \to \infty$ limit[6] as well as the singlet excitations out of the ground state in the Heisenberg chain.[3]

A. Imaginary part

The averaging via binning is obtained by replacing the delta function in Eq. (11) by a step function with an area of unity.

$$\mathrm{Im}\,\chi(q_z,\tilde\omega_j^{\rm inf} < \omega < \tilde\omega_j^{\rm sup}) = -\pi\sum_{m,n}\frac{f_{nm}(\beta)\,|V_{nm}|^2\,[\theta(\omega_{nm} - \tilde\omega_j^{\rm inf}) - \theta(\omega_{nm} - \tilde\omega_j^{\rm sup})]}{\tilde\omega_j^{\rm sup} - \tilde\omega_j^{\rm inf}} \tag{13}$$

$\theta(x)$ is the Heaviside function. For systems with well defined quasi-particle excitation spectra with spectral lines at frequencies $\tilde\omega_j$ as the XY-model or Heisenberg chains at $T = 0$, the appropriate choice is such that the interval boundaries lie in the middle between those spectral lines:

$$\tilde\omega_j^{\rm inf} = (\tilde\omega_{j-1} + \tilde\omega_j)/2\,, \tag{14}$$

$$\tilde\omega_j^{\rm sup} = (\tilde\omega_j + \tilde\omega_{j+1})/2\,. \tag{15}$$

Introducing the density of states η^{-1} with respect to Bethe-ansatz quantum numbers it can be shown[3,20,21] that for systems with well defined quasi-particle excitation spectra Eq. (11) can be represented scaled with the system size as

$$\mathrm{Im}\,\chi(q_z,\tilde\omega_j) = -\lim_{L\to\infty}\frac{L}{2}\,\eta[\tilde\omega_j]\sum_{m,n}^{\tilde\omega_j = E_n - E_m} f_{nm}(\beta)\,|V_{nm}|^2\,. \tag{16}$$

The sum covers only values of n and m such that $\tilde{\omega}_j = E_n - E_m$, L is the number of magnetic ions on a chain. Approximating the derivative in the density of states for a finite system as

$$\eta^{-1}[\tilde{\omega}_j] \approx \frac{1}{2}\,\frac{\tilde{\omega}_j - \tilde{\omega}_{j-1}}{2\pi/L} + \frac{1}{2}\,\frac{\tilde{\omega}_{j+1} - \tilde{\omega}_j}{2\pi/L} \tag{17}$$

Eq. (16) becomes

$$\operatorname{Im}\chi(q_z,\tilde{\omega}_j) = \sum_{m,n}^{\tilde{\omega}_j = E_n - E_m} \frac{-2\pi\ f_{nm}(\beta)\,|V_{nm}|^2}{\tilde{\omega}_{j+1} - \tilde{\omega}_{j-1}}. \tag{18}$$

Given the definitions Eqs. (14) and (15) the expressions (13) and (18) are identical, except for the latter being only defined at discrete frequencies. Both approaches suffer the disadvantage of ambiguity concerning the definition of the interval Eqs. (14) and (15) in one case and of the difference quotient Eq. (17) in the other. For larger system sizes,[3,20] where the density of spectral lines $\tilde{\omega}_j$ is much higher, this ambiguity becomes irrelevant.

For Heisenberg chains at finite temperatures the definition of the density of states η^{-1} with respect to Bethe-ansatz quantum numbers is inappropriate since a large number of spectral lines are present (see Sec. IV). The binning procedure Eq. (13) has to be applied. At higher temperatures the interval boundaries $\tilde{\omega}_j^{\mathrm{sup}} = \tilde{\omega}_{j+1}^{\mathrm{inf}}$ usually are chosen equidistantly.[5,4]

B. Real part

As can be seen from the denominator of Eq. (10) the real part of χ is divergent for frequencies $\omega \to E_m - E_n$. For arbitrarily small but finite ϵ the term which leads to the divergence at $\omega \sim \omega_{nm} = E_m - E_n$ vanished for $\omega = \omega_{nm}$.

$$0 = \left.\frac{(\omega + E_n - E_m)}{(\omega + E_n - E_m)^2 + \epsilon^2}\right|_{\omega=\omega_{nm}} \qquad \forall\ \epsilon \neq 0 \tag{19}$$

It turns out that for systems with well defined quasi-particle excitation spectra as the XY-model or Heisenberg chains at $T = 0$ and for an accordingly chosen set of frequencies $\{\tilde{\omega}_j\} = \{\omega_{nm}\}$ this allows a very accurate determination of the real part of the correlation function from Eq. (10).

In the case of Heisenberg chains at finite temperatures additional spectral lines stemming from transitions out of various thermally activated states are close to each other. This results in lack of accuracy since the frequencies $\tilde{\omega}_j$ chosen at $T = 0$ now lie uncontrolled on the shoulders of those additional spectral lines. This problem can be overcome by suppressing all contributions to the correlation function value in an interval $E_n - E_m \in [\tilde{\omega}_j \pm \Delta\omega]$.

$$\operatorname{Re}\chi(q_z,\tilde{\omega}_j) = \sum_{m,n} \frac{f_{nm}(\beta)\,|V_{nm}|^2}{(\tilde{\omega}_j + E_n - E_m)}\ \theta(|E_n - E_m - \tilde{\omega}_j| - \Delta\omega) \tag{20}$$

As discussed in the subsequent sections it turns out that for $\Delta\omega > 0.2J$ $\operatorname{Re}\chi(q_z,\tilde{\omega}_j)$ is a smooth function of $\Delta\omega$. For the Heisenberg chains discussed $\operatorname{Re}\chi(q_z,\tilde{\omega}_j)$ is constant for $0.06J < \Delta\omega < 0.13J$. At intermediate temperatures $0.1J < k_{\mathrm{B}}T < 0.9J$ the method yields inaccurate results for $\Delta\omega < 0.6J$ since the data points are located on shoulders of nearby divergences. At higher temperatures the finite size effects become negligible,[5] at lower temperatures the limiting value is given by the accuracy with which the $\tilde{\omega}_j$ are determined. I show that a choice of $\Delta\omega = 0.1J$ yields reliable results in all parameter regimes.

For higher frequencies the results for the real part of the correlation functions are free of finite size effects.

III. XY MODEL

I demonstrate the regularization method and its applicability for an exactly solvable case, the XY model. Neglecting the exchange between the $S_{\mathbf{l}}^z$ components of the spin system the magnetic Hamiltonian reduces to

$$H_s^{\mathrm{XY}} = J\ \sum_{\mathbf{l}} \left(S_{\mathbf{l}}^x S_{\mathbf{l}+\hat{z}}^x + S_{\mathbf{l}}^y S_{\mathbf{l}+\hat{z}}^y\right). \tag{21}$$

I have also neglected the next nearest neighbor coupling J_2. The dimer operator becomes

$$Y_{-\mathbf{q}}^{\mathrm{XY}} := \sum_{\mathbf{l}}\ e^{i\mathbf{q}\mathbf{R}_{\mathbf{l}}}\ \left(S_{\mathbf{l}}^x S_{\mathbf{l}+\hat{z}}^x + S_{\mathbf{l}}^y S_{\mathbf{l}+\hat{z}}^y\right). \tag{22}$$

A. Exact results

The spin operators in this model can be transformed to non-interacting, spin-less fermions via a Jordan-Wigner transformation.[22] The correlation function can then be determined in the thermodynamic limit.[13,14]

$$\chi_{\mathrm{XY}}(q_z,\omega) = \lim_{\substack{\epsilon\to 0\\ L\to\infty}} \frac{1}{2L}\sum_{k_z} \frac{[1+\cos(2k_z+q_z)c]\ \ [f_{k_z} - f_{k_z+q_z}]}{\omega + E_{k_z} - E_{k_z+q_z} + i\epsilon} \tag{23}$$

The energy dispersion is given by $E_{k_z} = J\cos(k_z c)$, f_{k_z} are Fermi distribution functions, the sum covers the first Brillouin zone, L is the number of magnetic ions in a chain. In general for $L \geq 10^4$ the result is independent of L for all practical purposes.

The imaginary part of Eq. (23) can be given for $q_z = \pi/c$ in closed form as[23]

$$-\operatorname{Im}\chi_{\mathrm{XY}}(\pi/c,\omega) = \frac{\sqrt{(2J)^2 - \omega^2}}{(2J)^2}\tanh\left(\frac{\beta\omega}{4}\right)\theta(2J - |\omega|). \tag{24}$$

In the limit $T \to 0$ the real part attains a simple form, too. Defining $x = \omega/(2J)$ one has for $|x| \leq 1$

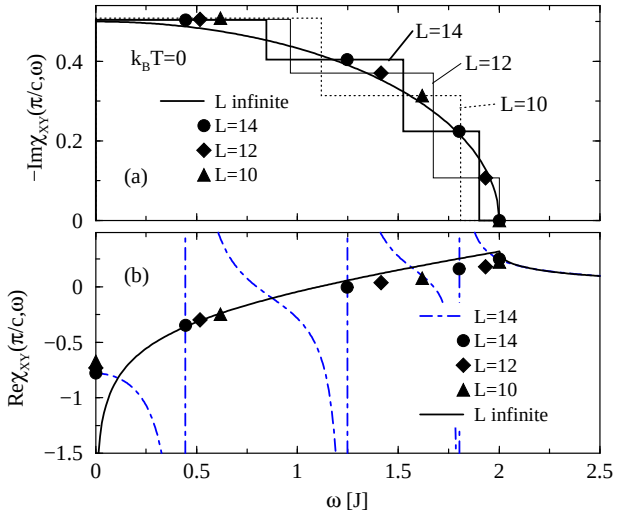

FIG. 1. *Dimer-dimer correlation function in the XY case at $T = 0$. (a) imaginary part, (b) real part. Thermodynamic limit results (full lines) are obtained via Eqs. (24) through (26). Step functions are binned as given in Eq. (13). Symbols are from Eq. (18) (imaginary part) and (23) (real part) at frequencies $\tilde{\omega}_j$. Finite size effects of the real part are largest at $\omega = 0$. Dash-dotted line: exact diagonalization from Eq. (10).*

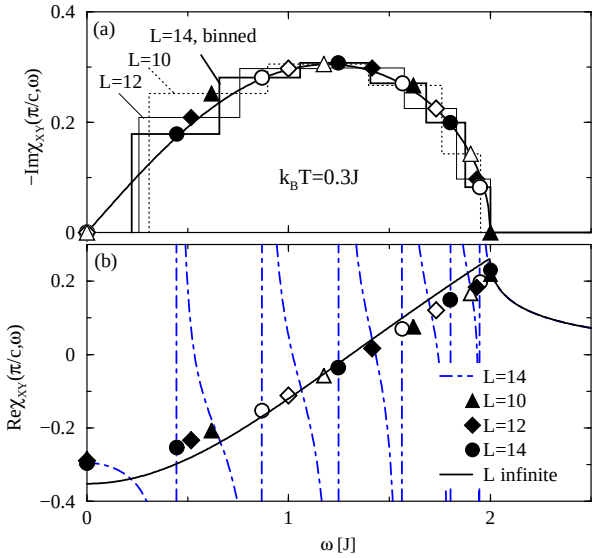

FIG. 2. *(a) Full line: imaginary part of the correlation function Eq. (24) at $k_{\rm B}T = 0.3J$. Step functions are binned as given in Eq. (13). Symbols are from Eq. (18). (b) Full line: real part of the correlation function Eq. (23) at $k_{\rm B}T = 0.3J$. Dash-dotted line: exact diagonalization from Eq. (10). Full symbols are values at the spectral lines $\tilde{\omega}_j \in \mathcal{W}_{\rm XY}^{(L)}$ present at $T = 0$, open symbols are additional spectral lines $\tilde{\mathcal{W}}_{\rm XY}^{(L)} \setminus \mathcal{W}_{\rm XY}^{(L)}$ at finite T.*

$$\mathrm{Re}\,\chi_{\rm XY}^{(0)}(\pi/c,\omega) = \frac{1}{\pi J} - \frac{\sqrt{1-x^2}}{\pi J}\ \ln\left|\frac{1+\sqrt{1-x^2}}{x}\right| \quad (25)$$

and for $|x| \geq 1$

$$\mathrm{Re}\,\chi_{\rm XY}^{(0)}(\pi/c,\omega) = \frac{1}{\pi J} - \frac{\sqrt{x^2-1}}{\pi J}\ \arcsin\left(1/x\right). \quad (26)$$

The imaginary part of the correlation function Eq. (23) is depicted for different temperatures by the solid lines in Figs. 1 and 2 (a), the real part in Figs. 1 and 2 (b).

B. Comparing finite and infinite systems

In finite systems with periodic boundary conditions the allowed wave vectors are $k_z(j) = 2\pi j/L$ for $L/2$ odd and $k_z(j) = \pi(2j+1)/L$ for $L/2$ even with $j \in \{0,\ldots,L-1\}$.[24] For $q_z = \pi/c$ at $T = 0$ the only spectral components contributing to the dimer-dimer correlation function Eq. (23) are fermion-hole excitations with $\tilde{\omega}_j = -2E_{k_z(j)}$ forming a well defined continuum in the thermodynamic limit and with excitations only within the half filled fermionic band.[6,25] In the example of $L = 14$ the values to consider are $\tilde{\omega}_j \in \mathcal{W}_{\rm XY}^{(14)}$, where $\mathcal{W}_{\rm XY}^{(14)} = J\{0.445, 1.247, 1.802, 2\}$.

In Fig. 1 I show different approaches to deduce the imaginary and real part of the dimer-dimer correlation function from finite systems compared with the exact result in the thermodynamic limit ($L \to \infty$, full lines) at $T = 0$. The step functions in Fig. 1 (a) resulting from the binning approach Eq. (13) approximate the exact curve quite satisfactorily, albeit with limited frequency resolution. The scaling approach from Eq. (18) also yields excellent agreement as shown by the symbols.

The dash-dotted line in Fig. 1 (b) is the result of the real part from Eq. (10) via exact diagonalization for 14 sites. Above the fermionic spectrum, i.e., $\omega > 2J$, the finite system gives a very accurate result. This is equivalent to the good agreement of the real time correlation functions from ED and $L \to \infty$ results for small time scales.[5] The symbols show the results using Eq. (10) by only regarding frequencies $\mathcal{W}_{\rm XY}^{(L)}$ and $\omega = 0$. The points give a satisfactory approximation of the exact curve in the thermodynamic limit. The discrepancies due to finite size effects are largest at $\omega = 0$.

At finite temperatures additional spectral lines are present, namely for all wave vectors $k_z(j) = \pi j/L$, albeit with temperature dependent weight. The additional excitations are fermion-hole like out of thermaly excited superpositions of states with a fermionic vacancy and an additional fermion $|\Phi_\pm\rangle = \sqrt{2}^{-1}(|L/2-1\rangle \pm |L/2+1\rangle)$. For $L = 14$ on has $\tilde{\omega}_j \in \tilde{\mathcal{W}}_{\rm XY}^{(14)}$ with $\tilde{\mathcal{W}}_{\rm XY}^{(14)} = J\{0.445, 0.868, 1.247, 1.564, 1.802, 1.950, 2\}$. This circumstance can be used to enhance the energy resolution of the calculations at finite temperatures. Since the spectral weight of the additional spectral lines is small at small temperatures, an application to the imaginary part will only yield reasonable results for $T \geq 0.3J$. Figure 2 (a) shows the excellent agreement with the exact

curve (full line) of both the binned step functions from Eq. (13) and the symbols of the scaling approach Eq. (18) using $\tilde{\mathcal{W}}_{\rm XY}^{(14)} \cup \{0\}$. Note that the application of the scaling approach is only possible here since I can take into account all spectral lines. $\omega = 0$ needs to be included in the spectrum because of the degeneracy of $|\Phi_+\rangle$ and $|\Phi_-\rangle$.

The calculation with the extended spectrum $\tilde{\mathcal{W}}_{\rm XY}^{(L)}$ can be applied to the real part in principle at any finite temperature, albeit with some small scattering of the data points at $k_{\rm B}T < 0.3J$ as shown for the Heisenberg cases in the subsequent sections. The continuous line in Fig. 2 (b) shows the real part of the correlation function Eq. (23) at $k_{\rm B}T = 0.3J$ for the XY model. The dash-dotted line is the result from Eq. (10) via exact diagonalization for 14 sites showing the spectral lines $\tilde{\omega}_j$ as divergences. For $\omega > 2J$ finite size effects are absent. The full symbols show the results using Eq. (10) by only regarding frequencies $\mathcal{W}_{\rm XY}^{(L)}$ as present at $T = 0$, open symbols are added at finite temperatures. The points give an excellent approximation of the exact curve in the thermodynamic limit.

IV. HEISENBERG MODEL

I now determine the dimer-dimer correlation function for Heisenberg chains with the Hamiltonian given in Eq. (3) in the case of $\alpha = J_2/J = 0$.

A. Zero temperature

At $T = 0$ the spectral lines $\tilde{\omega}_j \in \mathcal{W}_0^{(L)}$ at $q_z = \pi/c$ can be identified as the magnetization conserving (singlet) excitations out of the ground state determined via the Bethe ansatz, which form a well defined continuum in the thermodynamic limit.[1,2] Equation (18) can thus be applied and Eq. (10) can be regularized as discussed in Sec. II.

For a 16 site chain the four spectral lines at $\mathcal{W}_0^{(16)} = J\{0.446, 1.669, 2.588, 3.083\}$ lead to the imaginary part of the dimer-dimer correlation function as shown in Fig. 3 (a). The bins are obtained using Eq. (13) and the symbols are given using Eq. (18). The field theoretical prediction Eq. (6) reduces for $T \to 0$ to[6–8]

$$-\operatorname{Im}\chi_{\rm CF}^{(0)}(\pi/c,\omega) = \frac{C}{\omega}\,\theta(\Lambda - |\omega|)\,. \qquad (27)$$

From the fit (dashed line in Fig. 3 (a)) I conclude $C \approx 1$. The correspondece of the fit is not too good and suggests the presence of correction terms. The cut off parameter $\Lambda \approx \pi J$ is determined via the real part (see below) and indicates that the spectral weight lies mostly within the two-spinon continuum.[26,20]

The real part of the dimer-dimer correlation function is shown in Fig. 3 (b). For $\omega > \pi J$ the numerical results are in the thermodynamic limit showing the cut off to

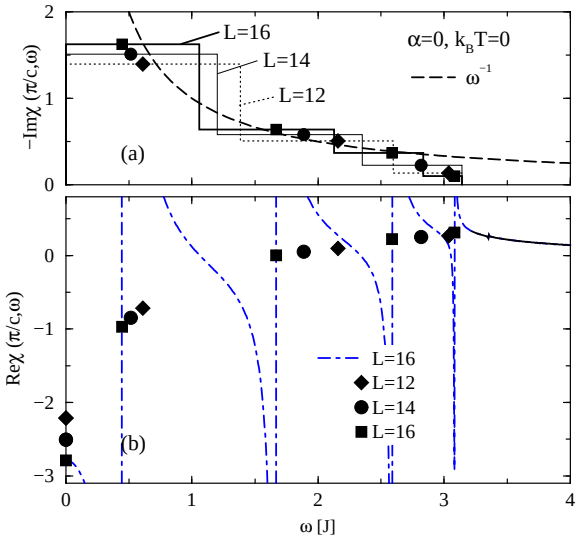

FIG. 3. *Imaginary part (a) and real part (b) of the dimer-dimer correlation function in the unfrustrated Heisenberg chain at $T = 0$. The imaginary part for finite systems is binned (Eq. (13)), each bin holds one spectral line, symbols are from Eq. (18). The dashed line is the field theoretical result (cf. Eq. (27)). The symbols for the real part as well as the dash-dotted line are obtained using Eq. (10), for $\omega > 3.14J$ the numerical result is in the thermodynamic limit (full line).*

be $\Lambda = \pi J$. For $\omega = 0$ finite size effects are significant since one expects from field theory and by analogy to the XY model $\operatorname{Re}\chi^{(0)}(\pi/c, \omega = 0) \to -\infty$. For $\omega \neq 0$ the field theoretical result obtained by the Kramers-Kronig transform of Eq. (27) is

$$\operatorname{Re}\chi_{\rm CF}^{(0)}(\pi/c,\omega \neq 0) = \frac{C}{\pi\omega}\,\ln\left|\frac{\Lambda+\omega}{\Lambda-\omega}\right| > 0 \qquad (28)$$

with a non-continuous jump to $\operatorname{Re}\chi_{\rm CF}^{(0)}(\pi/c, 0) = -\infty$. In contrast to that for $\omega < J$ the numerical data in Fig. 3 (b) indicate $\operatorname{Re}\chi^{(0)}(\pi/c,\omega) < \operatorname{Re}\chi_{\rm XY}^{(0)}(\pi/c,\omega) < 0$. This suggests significant corrections to the field-theoretical results Eq. (28) and (27).

B. Finite temperatures

At finite temperatures additional spectral lines attain significant weight as can be seen by the divergences in the real part of the correlation function Eq. (10) as plotted for $k_{\rm B}T = 0.1J$ in Fig. 4 (b) (dash-dotted line with L=16). The most dominant spectral lines are $\tilde{\mathcal{W}}_0^{(16)} = J\{0.446, 1.125, 1.669, 2.174, 2.588, 2.870, 3.083\}$.

The imaginary part of the dimer-dimer correlation function is determined via the same binning procedure as for $T = 0$ and shown in Fig. 4 (a). At $k_{\rm B}T = 0.1J$ the weight of the additional spectral lines $\tilde{\mathcal{W}}_0^{(16)} \setminus \mathcal{W}_0^{(16)}$ is too small to improve the frequency resolution as has been done in the XY case for $k_{\rm B}T = 0.3J$. The scaling

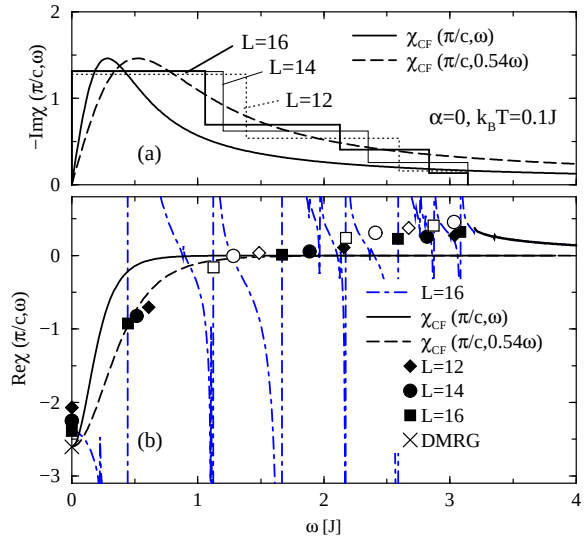

FIG. 4. *Imaginary part (a) and real part (b) of the dimer-dimer correlation function in the unfrustrated Heisenberg chain at $k_BT = 0.1J$. The imaginary part for finite systems is binned as in Fig 3. The real part for $\omega < 3.14J$ is obtained using $\Delta\omega = 0.1J$ and is given by full symbols at frequencies as for $T = 0$ and by open symbols at additional spectral lines appearing for $T > 0$. For $\omega > 3.14J$ the numerical result is in the thermodynamic limit (thick full line). The full lines are the Cross and Fisher result Eq. (6), the dashed lines are rescaled according to Eq. (29).*

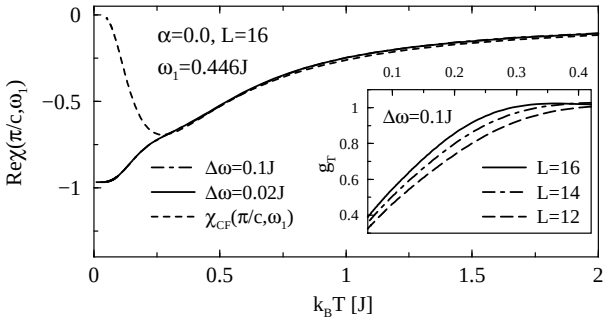

FIG. 5. *Temperature dependence of $\mathrm{Re}\,\chi(\pi/c,\omega_1)$ for $\omega_1 = 0.446J$: the result from Eq. (20) is practically independent of $\Delta\omega$, the lines for $\Delta\omega = 0.02J$ and $\Delta\omega = 0.1J$ fall on top of each other. The dashed line is the field-theoretical result $\mathrm{Re}\,\chi_{\mathrm{CF}}(q_z,\omega_1)$ from Eq. (6). The inset shows the scaling function defined in Eq. (29) for different chain lengths. The frequency corresponding to $L = 14$ is $\omega_1 = 0.516J$, for $L = 12$ it is $\omega_1 = 0.61J$.*

regularization Eq. (18) is inappropriate at finite temperatures in the Heisenberg model as discussed in Sec. II.

The real part of the correlation function has to be regularized according to Eq. (20). The resulting values for $\Delta\omega = 0.1J$ are shown by the symbols in Fig. 4 (b). Full symbols are evaluated at the $\tilde{\omega}_j \in \mathcal{W}_0^{(16)}$, open symbols are determined at additional dominant spectral lines and are less accurate. The finite size effects are of the order of 10% at $\omega = 0$ as can be seen by comparison with DMRG results in the thermodynamic limit[19] shown by the cross in Fig. 4 (b). They are negligible for $\omega > \pi J$.

The full lines in Fig. 4 (a) and (b) show the field-theoretical result $\chi_{\mathrm{CF}}(q_z,\omega)$ as given by Eq. (6). The functions are scaled by $\chi_0(k_BT/J)$ to match the $\omega = 0$ values obtained by DMRG.[19] Both real and imaginary part fit the numerical data better when rescaling the frequency dependence as $\chi_{\mathrm{CF}}(q_z,\omega \to 0.54\omega)$ (dashed lines in Fig. 4 (a) and (b)). The temperature dependence of the discrepancy between field-theory (dashed line) and numerical result for the real part (full line) at $\omega = \omega_1 = 0.446J$ is shown in Fig. 5.

As demonstrated in Fig. 5, the numerical result for $\mathrm{Re}\,\chi(\pi/c,\omega_1)$ with $\omega_1 = 0.446J$ is practically independent of $\Delta\omega$ for all temperatures. I use this circumstance to determine the scaling function g_T such that

$$\mathrm{Re}\,\chi_{\mathrm{CF}}(\pi/c, g_T\,\omega_1) = \mathrm{Re}\,\chi(\pi/c,\omega_1)\,. \qquad (29)$$

This procedure shows little finite size effects since the finite size scaling displaces the points at ω_1 along the slope of the fit function as can be seen in Fig. 4 (b). The resulting g_T is shown in the inset of Fig. 5. The results for different chain lengths show that $L = 16$ yields an upper bound for g_T, the finite size effects decrease with decreasing temperature.

The following arguments show the validity of the real-part results even for finite regularization parameters $\Delta\omega$:

(i) All symbols shown in Fig. 4 (b) follow a smooth line as expected by comparing with field-theoretical results and the XY model. The real part changes sign as a function of frequency as expected.

(ii) The dependence of $\mathrm{Re}\,\chi^{(0)}(\pi/c,\tilde{\omega}_j)$ on $\Delta\omega$ is small. This is shown for $\tilde{\omega}_j = \omega_1 = 0.446J$ in Fig. 5, where the the values of the correlation function for $\Delta\omega = 0.02J$ and $\Delta\omega = 0.1J$ fall on top of each other for all temperatures.

(iii) The scaling function g_T determined by $\mathrm{Re}\,\chi(\pi/c,\omega_1)$ also yields a better field-theoretical fit of the imaginary part of the correlation function.

V. FRUSTRATED HEISENBERG CHAIN

For $J_2 \neq 0$ the Heisenberg model is not integrable any more and thus the classification of the excitation spectrum at $T = 0$ is not possible from the Bethe ansatz. I discuss here a value of $\alpha = J_2/J = 0.24$ which is among the proposed ones for $CuGeO_3$[12,27] and is close the quantum critical point[28] making the field-theoretical result given in Eq. (6) eligible for comparison.

A. Zero temperature

The dash-dotted line in Fig. 6 (b) shows that at $T = 0$ for a 16 site chain there are four spectral lines $\tilde{\omega}_j \in \mathcal{W}_{.24}^{(16)} = J\{0.233, 1.174, 1.963, 2.403\}$ which, by

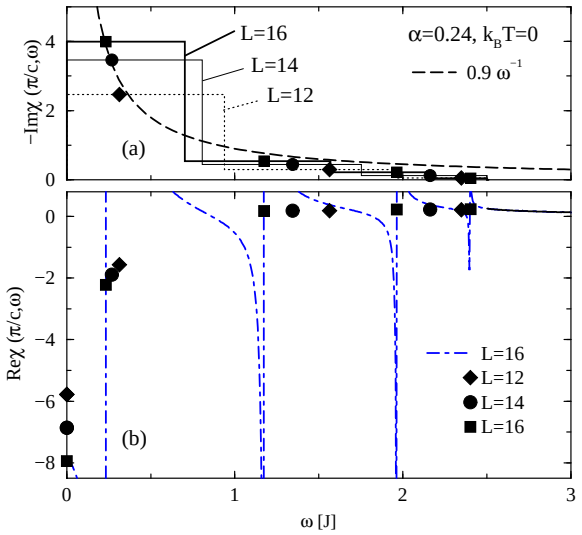

FIG. 6. *Imaginary part (a) and real part (b) of the dimer-dimer correlation function in the frustrated Heisenberg chain at $T = 0$ with $\alpha = 0.24$. The imaginary part for finite systems is binned (Eq. (13)), each bin hold one spectral line, symbols are from Eq. (18). The dashed line is the field-theoretical result (cf. Eq. (27)). The symbols for the real part as well as the dash-dotted line are obtained using Eq. (10), for $\omega > 2.5J$ the numerical result is in the thermodynamic limit (full line).*

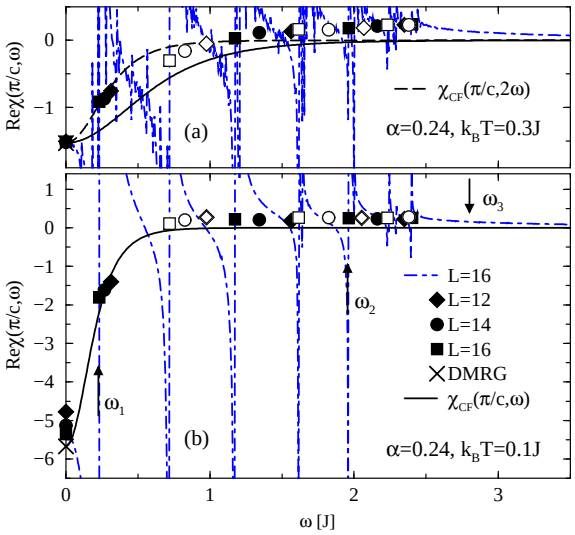

FIG. 7. *Real part of the dimer-dimer correlation function for $\alpha = 0.24$ at $k_BT = 0.1J$ (b) and $k_BT = 0.3J$ (a). Dash-dotted lines: results applying Eq. (10). Symbols: values obtained via Eq. (20) with $\Delta\omega = 0.1J$ for different system sizes. Full lines are the field-theoretical results from Eq. (6), the dashed line is the scaled result, see Eq. (29).*

analogy to the unfrustrated case, may also be identified as the singlet excitations out of the ground state. It is thus reasonable to suppose them to form a well defined continuum in the thermodynamic limit and thus Eqs. (18) and (10) can be applied ($\Delta\omega = 0$). Note that $|\mathcal{W}^{(L)}_{.24}| = |\mathcal{W}^{(L)}_{0}| = [L - L\mathrm{mod}(4)]/4$ for the chain lengths investigated.

The imaginary part of the dimer-dimer correlation function is shown in Fig. 3 (a). The bins are obtained using Eq. (13) and the symbols are given using Eq. (18). The fit to the field theoretical prediction Eq. (27) (dashed line in Fig. 6 (a)) leads to conclude $C = 0.9$. The cut off parameter $\Lambda \approx 2.5J$ determined via the real part (see below) indicates that the spectral weight lies mostly within a bounded continuum just as in the unfrustrated case.[29]

The real part of the dimer-dimer correlation function is shown in Fig. 6 (b). For $\omega > 2.5J$ the numerical results are in the thermodynamic limit suggesting the cut off to be $\Lambda = 2.5J$. For $\omega = 0$ finite size effects are significant since one expects from field theory and by analogy to the XY model $\mathrm{Re}\,\chi^{(0)}(\pi/c, \omega = 0) \to -\infty$.

The agreement with the field-theoretical results Eqs. (27) and (28) is better than in the unfrustrated case but the analogy to the XY model again suggests $\mathrm{Re}\,\chi^{(0)}(\pi/c, 0.233J) < 0$. It cannot be entirely excluded though that the discrepancy is due to finite size effects.

B. Finite temperatures

At finite temperatures additional spectral lines attain significant weight as can be seen by the divergences in the real part of the correlation function Eq. (10) as plotted for $k_BT = 0.1J$ in Fig. 7 (b) and for $k_BT = 0.3J$ in Fig. 7 (a) (dash-dotted lines with L=16). The most dominant and thus relevant spectral lines are $\tilde{\omega}_j \in \tilde{\mathcal{W}}^{(16)}_{.24} = J\{0.233, 0.720, 1.174, 1.616, 1.963, 2.232, 2.403\}$. Again, the analogy to the unfrustrated Heisenberg chain is obvious since $|\tilde{\mathcal{W}}^{(L)}_{.24}| = |\tilde{\mathcal{W}}^{(L)}_{0}|$ for the chain lengths investigated.

The imaginary part of the dimer-dimer correlation function is determined for $k_BT = 0.1J$ via the same binning procedure as for $T = 0$ and is shown in Fig. 8 (b). For $k_BT = 0.3J$ the set of frequencies given by $\tilde{\mathcal{W}}^{(16)}_{.24} \cup \{0\}$ enhancing the resolution as in the XY case. The resulting step functions from the binning procedure Eq. (13) are shown in Fig. 8 (a). In both cases the scaling regularization Eq. (18) is inappropriate as discussed in Sec. II.

The symbols in Fig. 7 (a) and (b) show the numerical results of the real part of the dimer-dimer correlation function applying Eq. (20) for $k_BT = 0.3J$ and $k_BT = 0.1J$, respectively, with $\Delta\omega = 0.1J$. The full symbols are at spectral lines $\mathcal{W}^{(L)}_{.24}$ and at $\omega = 0$, the open symbols are at $\tilde{\mathcal{W}}^{(L)}_{.24} \setminus \mathcal{W}^{(L)}_{.24}$.

For $\omega > 2.5J$ the numerical results in Fig. 7 are in the thermodynamic limit. The multitude of spectral lines appearing at finite temperatures which lead to the requirements on $\Delta\omega$ can clearly be seen by the

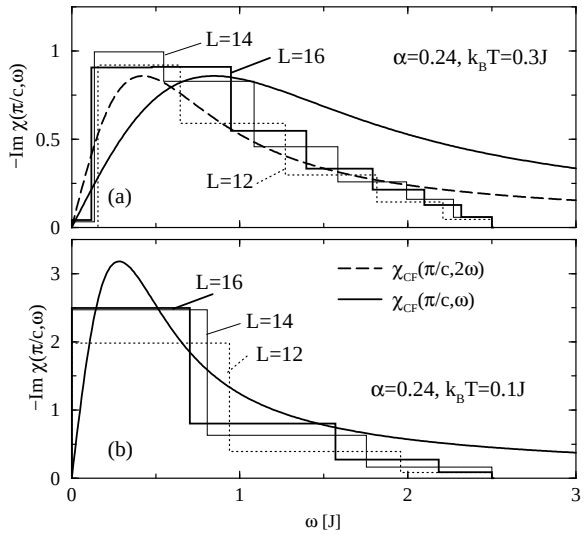

FIG. 8. *Imaginary part for $k_{\rm B}T = 0.1J$ and $k_{\rm B}T = 0.3J$ in the frustrated Heisenberg chain. Binned curves from Eq. (11), dashed lines from field theory Eq. (6), the dashed line is rescaled as in Fig. 7.*

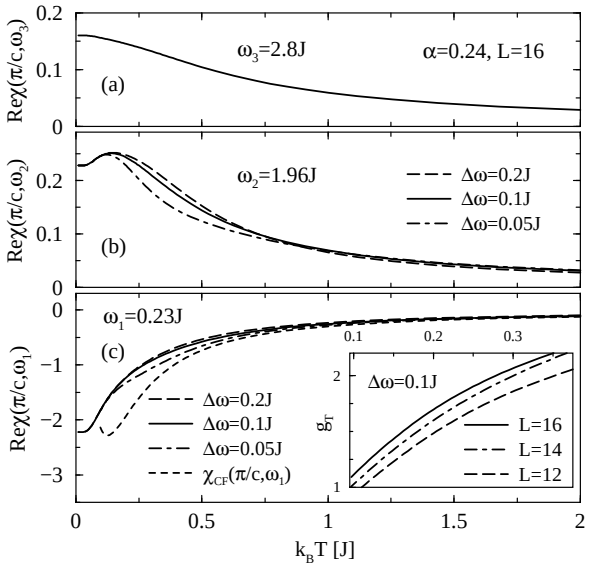

FIG. 9. *Temperature dependence of $\mathrm{Re}\,\chi(\pi/c,\omega_i)$ for ω_i as indicated in Fig. 7. (a) $\omega_3 = 2.8J$: result from Eq. (10). (b) $\omega_2 = 1.96J$ and (c) $\omega_1 = 0.23J$: results from Eq. (20), influence of $\Delta\omega$. For $\Delta\omega = 0.05J$ the points in Fig. 7 scatter significantly at intermediate temperatures, the results are reliable for $0.06J < \Delta\omega < 0.15J$. The short-dashed line in (c) is the field-theoretical result Eq. (6) deviating significantly for $k_{\rm B}T < 0.6J$. The inset shows the scaling function defined in Eq. (29) for different chain lengths. The frequency at $L = 14$ is $\omega_1 = 0.27J$ and at $L = 12$ it is $\omega_1 = 0.31J$.*

dash-dotted lines in Fig. 7 (a) and (b). To obtain the smooth results of the regularized data points a choice of $0.06J < \Delta\omega < 0.15J$ is necessary at intermediate temperatures $0.1J < k_{\rm B}T < 0.9J$.

The temperature dependent effect of the choice of $\Delta\omega$ is shown in Fig. 9 for three different frequencies. At $\omega_3 = 2.8J$ the result is equal to the thermodynamic limit. At intermediate frequencies, as shown in the example of $\omega_2 = 1.96J$ and $\omega_1 = 0.23J$ in Fig. 9 (b) and (c), respectively, values of $\Delta\omega < 0.06J$ and $\Delta\omega > 0.15J$ deviate from the best choice of $\Delta\omega < 0.1J$. For other temperatures, i.e., $0.1J > k_{\rm B}T$ and $k_{\rm B}T > 0.9J$, one may choose $\Delta\omega$ as small as $0.01J$. The influence of finite size effects can be estimated by comparing the $\omega = 0$ values with DMRG results shown by crosses in Fig. 7.[19] Together with the above discussed small dependence of the values on $\Delta\omega$ this is strong evidence for the accuracy of the results.

The field-theoretical result in Eq. (6) is expected to well describe the low energy physics. The full lines in Fig. 7 show the corresponding curves. The functions are scaled by $\chi_0(k_{\rm B}T/J)$ to match the $\omega = 0$ values obtained by DMRG.[19] While at $k_{\rm B}T = 0.1J$ both the imaginary and the real part of the dimer-dimer correlation function are well described for $\omega \leq J$ as shown in Figs. 8 and 7 (b), at $k_{\rm B}T = 0.3J$ the discrepancy to the numerical result is obvious as shown in Figs. 8 and 7 (a).

As in the unfrustrated case I attempt to improve the field-theoretical result by introducing the scaling function g_T defined in Eq. (29). The relevant frequency in the frustrated case is $\omega_1 = 0.23J$ for $L = 16$. The temperature dependence of $\chi(\pi/c, \omega_1)$ is depicted by the full line in Fig. 9 (c) in comparison to field theory (short-dashed line). The scaling function g_T is shown in the inset of Fig. 9 (c). The dashed line in Fig. 8 (a) shows the rescaled imaginary part of the rescaled field theoretical curve, the dashed line in Fig. 7 (a) shows the real part at $k_{\rm B}T = 0.3J$. Both fit the numerical data better than the unscaled result (full lines). Above $k_{\rm B}T > 0.3J$ the field-theoretical function Eq. (6) is not a good fit function any more since intermediate frequency values are underestimated.

In the temperature window $0.1J < k_{\rm B}T < 0.3J$ relevant for describing the quasi-elastic scattering in $CuGeO_3$ the above described fitting procedure is sufficiently accurate. More precise results for the correlation function can be obtained by fitting a spline to the spectrum of the real part and simultaneaously fitting its Kramers-Kronig transform to the imaginary part.

VI. APPLICATION TO CUGEO$_3$

$CuGeO_3$ undergoes a spin-Peierls transition at $T_{\rm SP} = 14.3$ K or $k_{\rm B}T_{\rm SP} \approx 0.1J$. The wave vector of the modulation in the ordered phase is $\mathbf{q}_0 = (\pi/a, 0, \pi/c)$, where a and c are the lattice constant along the crystallographic x and z direction, respectively. I set $J/k_{\rm B} = 150$ K which is together with a value of $J_2/J = 0.24$ among those discussed as valid for $CuGeO_3$.[12,27]

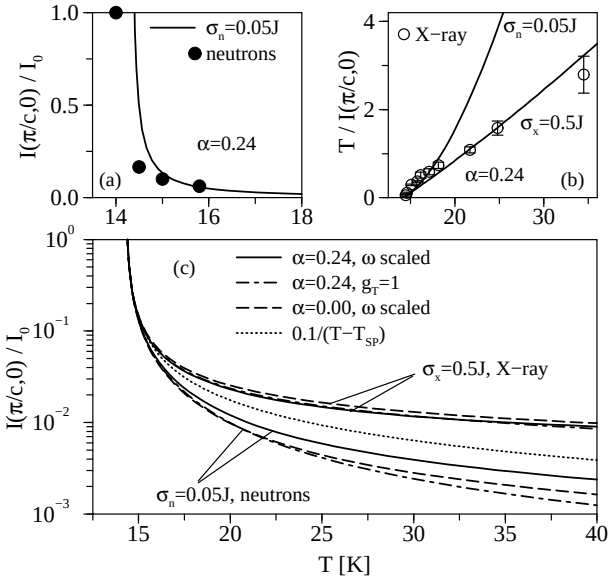

FIG. 10. *Intensity of quasi-elastic scattering. (a) The fast drop* $I \sim (T-T_{\rm SP})^{-1}$ *above the phase transition at* $T_{\rm SP} = 14.3$ *K is basically independent of the choice of parameters and matches the data from neutron scattering (filled circles, Ref. 15). (b) The curve of* $T/I(\mathbf{q}_0, 0)$ *obtained with the larger resolution* $\sigma_x = 0.5J$ *match the X-ray data (open circles, scaled, Ref. 17) better than that obtained with* $\sigma_n = 0.05J$*. (c) The influence of the choice of parameters shown on a logarithmic scale. For* $\sigma_x = 0.5J$ *the curves lie up to an order of magnitude higher than for* $\sigma_n = 0.05J$*. The dot-dashed lines show the effect of omitting the frequency scaling (*$g_T \equiv 1$*). The dashed curves show the effect of the different functional dependence of* $\chi_0(k_{\rm B}T/J)$ *in Eq. (6) for* $\alpha = J_2/J = 0$*.*

A. Quasi-elastic scattering

Quasi-elastic scattering has been observed in X-ray scattering up to 40 K or $k_{\rm B}T \approx 0.3J$.[17] I can thus use the results presented in Sec. V to compare with experiment. In neutron scattering experiments the quasi-elastic scattering is observable only up to 16 K.[16,15]

The frequency dependent scattering rate of inelastic neutrons or X-rays can be obtained by convoluting the dynamical structure factor (1) with a Gaussian of the width of the experimental resolution σ.

$$I(\mathbf{q}_0, \omega) = \frac{1}{\sqrt{2\pi}\sigma} \int_{-\infty}^{\infty} \mathrm{e}^{-\frac{(\omega'-\omega)^2}{2\sigma^2}}\ S(\mathbf{q}_0, \omega')\ d\omega' \qquad (30)$$

The energy resolution in neutron scattering is of the order of a few meV while X-rays integrate over a much larger energy interval. $\sigma = \sigma_n \approx 0.05J$ simulates the resolution of diffracted neutrons[10] and $\sigma = \sigma_x \approx 0.5J$ is relevant for X-ray scattering. The X-ray resolution is probably even larger, but the interval of $-0.5J < \omega < 0.5J$ covers the full width of the relevant magnetic spectrum, compare Fig. 7. Also, the fit function Eq. (6) is not reliable for $|\omega| > J$.

Fig. 10 (a) shows the fast drop of the intensity of the quasi-elastic scattering above the phase transition. The theoretical intensity (full line) is normalized with $I_0 = I(\mathbf{q}_0, 0)|_{T=14.4\,\rm K}$. It is basically independent of the choice of parameters, all curves shown in Fig. 10 (c) fall more or less on the same line on the linear scale.

The full curve in Fig. 10 (a) matches the data from neutron scattering (filled circles, Ref. 15). Note that the critical region has been estimated via the Ginzburg criterion[12] to be $T_{\rm SP} \pm 0.4$ K. Within this region the theoretical divergence of the intensity $I = S(\mathbf{q}_0, 0) \sim (T-T_{\rm SP})^{-1}$ (dotted line in Fig. 10 (c)) will be suppressed by critical fluctuations. A more quantitative analysis also must include the limited momentum resolution of the neutron data as discussed in Ref. 14.

Fig. 10 (b) shows a plot of $T/I(\mathbf{q}_0, 0)$. As desired, the curve obtained with the larger resolution $\sigma_x = 0.5J$ match the X-ray data (open circles, scaled, Ref. 17) better than that obtained with $\sigma_n = 0.05J$.

The influence of the choice of parameters becomes apparent on the logarithmic scale shown in Fig. 10 (c). For $\sigma_x = 0.5J$ the curves lie an order of magnitude higher than for $\sigma_n = 0.05J$ at large temperatures. This explains why the correlation length can be extracted to higher temperatures from X-ray measurements[17] then from neutron scattering.[16] The dot-dashed lines show the effect of omitting the frequency scaling ($g_T \equiv 1$). For $\sigma_n = 0.05J$ the intensity is suppressed since the imaginary part without rescaling has less weight in the low energy regime (see Fig. 8 (a)). For $\sigma_n = 0.5J$ this effect is cancelled by the larger contribution of the real part (Fig. 7 (a)). The dashed curves show the effect of the different functional dependence of $\chi_0(k_{\rm B}T/J)$ in Eq. (6) for $\alpha = J_2/J = 0$.[19]

Overall, the effect of energy resolution accounts for the largest effects in the temperature dependence of the intensity of the quasi-elastic scattering. The effect of the frequency scaling g_T is a minor correction. Both neutron and X-ray scattering intensities are satisfactorily described within RPA.

B. Phonon hardening

The optical zone-boundary phonons coupling to the spin chains in $CuGeO_3$ have been shown to harden with the lowering of temperature.[18] The phononic excitations in RPA are essentially given by the roots of the real part of the denominator of the normal coordinate propagator.[10,13,14]

$$\mathrm{Re}\,\chi(\mathbf{q}, \omega) = \Big[\sum\nolimits_{\nu} g_{\nu,\mathbf{q}} g_{\nu,-\mathbf{q}}\ D_{\nu}^{(0)}(\mathbf{q}, \omega)\Big]^{-1} \qquad (31)$$

The coupling constants and bare phonon frequencies are given in Ref. 12. The Peierls-active phonon mode coupling strongest being $\Omega_{2,\mathbf{q}_0} = 2.13J$, the left hand side of Eq. (31) can be approximated by $\mathrm{Re}\,\chi(\mathbf{q}, 1.96J)$ as calculated in Sec. V.

The resulting temperature evolution is up to a prefactor and a constant given by Fig. 9 (b). In contrast to

the case of determining the dimer-dimer correlation function by the field-theoretical result Eq. (6),[10] the phonon hardens with decreasing temperature while $k_{\rm B}T > 0.2J$. This is reminiscent of the change of sign of the real part of the dimer-dimer correlation function discussed in Sec. V. The temperature evolution is in qualitative agreement with the experimental data from Ref. 18, but the phonon hardens only by 1% which is less than what is experimentally observed. The higher Peierls-active phonon modes show no spin-phonon coupling induced temperature dependence both in experiment and theory.

VII. CONCLUSIONS

Within the energy resolution limited by finite system sizes the dimer-dimer correlation functions obtained by exact diagonalization yield satisfactory approximations to the thermodynamic limit. This is supported by the comparison with the exact results for the XY model. The determination of both the real and the imaginary part yields an essential improvement of the reliability of the results.

The quantitative applicability of field-theoretical results for the dimer-dimer correlation functions is drawn into doubt, even at low frequencies and temperatures. At intermediate temperatures they can be used as fit functions by appropriately rescaling the amplitude and frequency dependence.

The intensity of the quasi-elastic scattering in $CuGeO_3$ is satisfactorily reproduced within the RPA approach. The impact of the energy resolution of the experimental setup on the temperature dependence of the quasi-elastic scattering has been shown. The numerical results yield the correct qualitative temperature dependence of the Peierls-active phonons.

VIII. ACKNOWLEDGMENTS

I thank K. Fabricius for calculating the matrix elements for system size 16 and instructive discussions. I thank M. Karbach and G. Müller for the excitation data from Bethe ansatz and extensive discussions on regularization procedures. I owe thanks to M. Braden for furnishing the neutron scattering data files and R. Raupach for the DMRG data files. I thank M. Braden, V. J. Emery, A. Klümper, S. Maslov, and R. Raupach for fruitful discussions. The work performed in Wuppertal was supported by DFG program "Schwerpunkt 1073", the work at BNL was supported by DOE contract number DE-AC02-98CH10886.

[1] M. Karbach and G. Müller, Comp. in Phys. **11**, 36 (1997).
[2] M. Karbach and G. Müller, Comp. in Phys. **12**, 565 (1998).
[3] M. Karbach, K. Hu, and G. Müller, to appear in Comp. in Phys. (2000).
[4] O. A. Starykh, A. W. Sandvik, and R. R. P. Singh, Phys. Rev. B **55**, 14953 (1997).
[5] K. Fabricius, U. Löw, and J. Stolze, Phys. Rev. B **55**, 5833 (1997).
[6] G. Müller, H. Thomas, H. Beck, and J. C. Bonner, Phys. Rev. B **24**, 1429 (1981).
[7] H. J. Schulz, Phys. Rev. B **34**, 6372 (1986).
[8] A. M. Tsvelik, *Quantum field theory in condensed matter physics* (Cambridge University Press, Cambridge, 1995).
[9] M. C. Cross and D. S. Fisher, Phys. Rev. B **19**, 402 (1979).
[10] C. Gros and R. Werner, Phys. Rev. B **58**, R14677 (1998).
[11] A. Klümper, R. Raupach, and F. Schönfeld, Phys. Rev. B **59**, 3612 (1999).
[12] R. Werner, C. Gros, and M. Braden, Phys. Rev. B **59**, 14356 (1999).
[13] R. Werner, *The spin-Peierls transition in $CuGeO_3$* (Ph.D. thesis, Dortmund, 1999), http://eldorado.uni-dortmund.de:8080/FB2/ls8/forschung/1999/werner.
[14] M. Holicki, H. Fehske, and R. Werner, preprint (2000).
[15] M. Braden, *Quantitative Analyse einer magnetoelastischen Kopplung am Beispiel von $CuGeO_3$* (Habilitation, Aachen, 1999).
[16] K. Hirota *et al.*, Phys. Rev. B **52**, 15412 (1995).
[17] J. P. Schoeffel, J. P. Pouget, G. Dhalenne, and A. Revcolevschi, Phys. Rev. B **53**, 14971 (1996).
[18] M. Braden *et al.*, Phys. Rev. Lett. **80**, 3634 (1998).
[19] R. Raupach, A. Klümper, and F. Schönfeld, preprint, cond-mat/9908407 (1999).
[20] M. Karbach and K.-H. Mütter, Preprint (2000).
[21] M. Karbach, private communication.
[22] E. F. Fradkin, *Field Theories of Condensed Matter Systems* (Addison-Wesley, New York, 1991).
[23] Y. Yu, G. Müller, and V. Viswanath, Phys. Rev. B **54**, 9242 (1996).
[24] E. Lieb, T. Schulz, and D. Mattis, Ann. Phys. **16**, 407 (1961).
[25] J. H. Taylor and G. H. Müller, Physica **130A**, 1 (1985).
[26] J. des Cloizeaux and J. J. Pearson, Phys. Rev. **128**, 2131 (1962).
[27] W. Brenig, Phys. Rev. B **56**, 14441 (1997).
[28] R. Chitra *et al.*, Phys. Rev. B **52**, 6581 (1995).
[29] For a frustration of $\alpha = 0.35$ the numerical analysis shows the cut off to be $\Lambda \approx 2.1J$. The effect of frustration is thus to compactify the dominant spectrum.